Cellular Signalling 123 (2024) 111350

Contents lists available at ScienceDirect

Cellular Signalling

journal homepage: www.elsevier.com/locate/cellsig

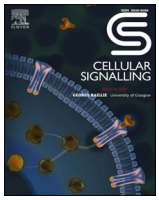

Atmospheric pressure plasma preconditioning reduces oxygen and glucose deprivation induced human neuronal SH-SY5Y cells apoptosis by activating protective autophagy and ROS/AMPK/mTOR pathway

Xu Yan [a,1,*], Yuqing Liu [b,1], Xi Zhang [a,1], Qi Zhang [d], Yixiao Liu [a], Yuqi Guo [a], Zhongfang Shi [a], Lixin Xu [a], Zilan Xiong [e,**], Jiting Ouyang [b,***], Ye Chen [a,c,*], Kostya (Ken) Ostrikov [f]

[a] Department of Pathophysiology, Beijing Neurosurgical Institute/ Beijing Tiantan Hospital, Capital Medical University, Beijing 100070, People's Republic of China
[b] School of Physics, Beijing Institute of Technology, Beijing, People's Republic of China
[c] Department of Pathology, Beijing Friendship Hospital, Capital Medical University, National Clinical Research Center for Digestive Diseases, Beijing 100050, China
[d] Ultrastructural pathology department, Beijing Neurosurgical Institute/ Beijing Tiantan Hospital, Capital Medical University, Beijing 100070, People's Republic of China
[e] State Key Laboratory of Advanced Electromagnetic Technology, Huazhong University of Science and Technology, Wuhan, Hubei 430074, People's Republic of China
[f] School of Chemistry and Physics and Centre for Biomedical Technologies, Queensland University of Technology, Brisbane, Queensland 4000, Australia

ARTICLE INFO

Keywords:
Atmospheric pressure plasma
RONS
Neuroprotection
Autophagy
ROS/AMPK/mTOR pathway

ABSTRACT

Reactive oxygen species (ROS)/reactive nitrogen species (RNS) exert a "double edged" effect on the occurrence and development of ischemic stroke. We previously indicate that atmospheric pressure plasma (APP) shows a neuroprotective effect in vitro based on the ROS/RNS generations. However, the mechanism is still unknown. In this work, SH-SY5Y cells were treated with oxygen and glucose deprivation (OGD) injuries for stimulating the ischemic stroke pathological injury process. A helium APP was used for SH-SY5Y cell treatment for evaluating the neuroprotective impacts of APP preconditioning against OGD injuries with the optimized parameters. During the preconditioning, APP significantly raised the extracellular and intracellular ROS/RNS production. As a result, APP preconditioning increased SH-SY5Y cell autophagy by elevating LC3-II/LC3-I ratio and autophagosome formation. Meanwhile, APP preconditioning reduced cell apoptosis caused by OGD with the increased APP treatment time, which was abolished by pretreatment with autophagy inhibitor 3-methyladenine (3-MA). The ROS scavenger *N*-acetyl-L-cysteine (NAC) alone or combined with NO scavenger carboxy-PTIO abolished the APP preconditioning induced SH-SY5Y autophagy and the cytoprotection, whereas the NO scavenger alone did not. In addition, we observed the elevated phosphorylation of AMP-activated protein kinase (AMPK) and decreased phosphorylation of mammalian target of rapamycin (mTOR) in APP treated SH-SY5Y cells. This effect was attenuated by AMPK inhibitor Compound C (CC), the ROS scavenger NAC and autophagy inhibitor 3-MA. Furthermore, the cytoprotective effect of APP was preliminarily confirmed in the rats of middle cerebral artery occlusion (MCAO) model. Results showed that APP inhalation by rats during MCAO process could improve neurological functions, reduce cell apoptosis in brain tissues and decrease cerebral infarct volume. Our data suggested that ROS produced by APP preconditioning played a vital role in the neuroprotective effect of SH-SY5Y cells against OGD injuries by activating autophagy and ROS/AMPK/mTOR pathway.

* Corresponding authors at: Department of Pathophysiology, Beijing Neurosurgical Institute/ Beijing Tiantan Hospital, Capital Medical University, Beijing 100070, People's Republic of China.
** Corresponding author.
*** Corresponding author.
E-mail addresses: devil-yx@163.com, yanxu@bjtth.org (X. Yan), zilanxiong@hust.edu.cn (Z. Xiong), jtouyang@bit.edu.cn (J. Ouyang), chenye940609@163.com (Y. Chen).
[1] Xu Yan, Yuqing Liu and Xi Zhang equally contributed to this work.

https://doi.org/10.1016/j.cellsig.2024.111350
Received 21 May 2024; Received in revised form 1 August 2024; Accepted 14 August 2024
Available online 19 August 2024

1. Introduction

Ischemic stroke mainly results from the interrupted cerebral blood flow, which is induced by the stenosis or obstruction of the cerebral artery lumen with thrombosis or embolism, and accounts for a major reasons for disability and mortality in adults globally [1,2]. Immediate clinical interventions, including intravenous thrombolytic treatment and mechanical thrombectomy, cause cerebral vascular recanalization, which is one of the most effective therapy method for ischemic stroke [3]. However, due to the irreversible damage and necrosis of brain tissue, the prognosis of some patients is still very poor although receiving reperfusion therapies [4]. Pharmacological treatments for ischemic stroke are restricted, indicating that it is necessary to develop novel approaches. Here we address this issue by using autophagy and the effective plasma-based mechanism of reactive oxygen/nitrogen species (ROS)/reactive species (RNS)generation.

Autophagy represents the evolutionarily conserved cellular process and is capable of degrading a variety of biological components (e.g., DNA, RNA, protein, glycogen, and lipids) and organelles (e.g., mitochondria, endoplasmic reticulum, ribosomes, lysosomes, and micronuclei) via the lysosomal pathway [5]. Although excessive autophagy can cause dysfunction of the corresponding cellular tissues, which in turn can develop into various clinical diseases, there are also numerous studies indicating that activation of autophagy could increases tolerance to ischemic injuries and reduces cell apoptosis in multiple tissues [6]. Previous studies have shown that autophagy could promote cardiomyocyte and hepatocyte survival during ischemia-reperfusion injuries [7,8]. In central nervous system, it is shown that autophagy is accompanied with cerebral ischemia, and contributes to neuronal dysfunction and neurodegeneration [9]. Meanwhile, accumulating evidence has suggested that the regulation of autophagy by RONS is an effective pathway for suppressing neuronal death and ameliorating cell damage [10]. But how autophagy affects ischemic stroke is still unclear and may exert both protective and/or detrimental impacts as a “double-edged sword”.

“plasma” here refers to an ionized gas, which is the fourth state of matter, and plasma is a macroscopic system that exhibits quasi-electrical neutrality in an unbound state [11]. The plasma emissions include free electrons, atoms, and molecules in neutral, ionized, and/or excited states, which can directly react with oxygen and nitrogen in the air to form multiple types of reactive ROS/RNS (such as O·, $O(^1D)$·, O_2^-·, ·OH, HO_2·, NO·, NO_2·, NO_3· and so on), since APP is generated under atmospheric environment [12]. For over two decades, atmospheric-pressure plasma (APP) has been proved effective on the inactivation of microorganisms [13], and other biomedical processes collectively creating the emerging interdisciplinary field of “plasma medicine” [14]. The application of plasma medicine has also gradually expanded from disinfection and sterilization to areas such as hemostasis and coagulation, oral medicine, cancer treatment, dermatology, and more [15,16]. Atmospheric pressure plasma jet (APPJ) is currently a widely used plasma source in plasma medicine due to its numerous advantages such as the ability to be generated in open spaces, ease of operation, high electron temperature, low gas temperature, and rich content of reactive species. Among them, ROS and RNS can participate in a series of biological activities and are considered as the main effectors of plasma on biological cells or tissues [17,18].

Previous scholars have demonstrated that APP protects neuronal cells against multiple injuries in vitro [19–21] and in a rat model with ischemic brain damages [22,23]. However, the underlying mechanisms, in particular the impactes of RONS are still unknow. In this work, SH-SY5Y human neuroblastoma cells, a commonly used cell line for neuroprotective studies with neuron-like characteristics, were cultured and treated with APP for different durations. Cell autophagy was detected and related to RONS generation. Cells were then treated with oxygen and glucose deprivation (OGD) to mimic the ischemic stroke induced neuronal cell damages. Cell viability, apoptosis, as well as the intracellular and extracellular reactive species were further evaluated. Meanwhile, cytoprotective effect of APP on MCAO rats was also confirmed. The mechanisms of neuroprotective effects of APP treatment are associated with the ROS/APMK/mTOR pathway, and ROS is necessary for the protection of damaged neuronal cells at the initial stage.

2. Materials and methods

2.1. SH-SY5Y cell culture

SH-SY5Y cells were purchased from the China Center for Type Culture Collection, Beijing, China. Cells were kept in RPMI-1640 medium (HyClone, Thermo Scientific) that contained 15% fetal calf serum (Gibco, Thermo Scientific), 100 U/ml penicillin and 100 U/ml streptomycin at 37 °C in a humidified incubator with 5% CO2 and 95% air. Logarithmic growth cells (4×10^5 cells/ml) were seeded into the 6-well plates for further experiments.

2.2. APPJ device and treatment

Fig. 1(a) displays the sketch map for experimental setup and more details of our APPJ device can be found in our previous studies [19]. APP was generated by a needle-ring dielectric barrier helium (He) discharge. The plasma was generated between the high voltage (HV) electrode and ground electrode by helium (He) gas discharge. The experimental voltage was 5.6 kV, the frequency was 5 kHz, and the helium flow rate was controlled at 1400 sccm by the mass flow controller (MFC, SevenStarCS200). The plasma plume was sprayed out from the quartz tube for cell treatment and rat inhalation. The emission spectra of APP were monitored by a four-channel fiber optical emission spectrometer (AvaSpec-ULS3648). Cells were seeded in the 6-well plates and placed under the nozzle of APPJ device. The distance between the nozzle of the quartz tube and the platform was adjusted to 2.5 cm so that the plasma beam could touch the surface of the culture medium.

2.3. Preparation of the OGD injury model of SH-SY5Y cells

Based on the protocols detailed previously, OGD condition was established for simulating the cell injuries processes in ischemic stroke [20]. Cells were pretreated with autophagy inhibitor 3-Methyladenine (3-MA) (10 mM, Sigma-Aldrich, USA), ROS scavenger *N*-acetyl-L-cysteine (NAC) (2.5 mM, Beyotime, Haimen, China), RNS scavenger carboxy-PTIO (200 μM, Beyotime, Haimen, China) and the AMPK inhibitor compound C (CC) (7.5 μM, Sigma-Aldrich) for 1 h before APP treatment. Cells treated with or without the inhibitors were cultured for another 1 h after the APP treatment. Fresh culture medium was added to replace the original one. Then, cells were subjected to additional 6-h incubation. Later, glucose-free 1640 (cat. Number 11879020, Gibco, Grand Island, USA) was added to remove the original medium, for the sake of achieving OGD condition. Later, cells were put into the tri-gas incubator (Binder, Germany) to automatically adjust gas composition into hypoxic condition through N_2 injection (0.2% O_2, 5% CO_2, 94.8% N_2). Normoxic condition was prepared for the control plates for a certain time period. At 18-h later, we collected cells to perform later analyses.

2.4. Cell viability assay

Lactate dehydrogenase (LDH) amount released into culture supernatants was detected for assaying cell injury. The LDH assay kit was used to identify LDH release of diverse groups according to corresponding protocols (Applygen Technologies Inc., Beijing, China). A microplate reader (M200 Pro, Tecan, Switzerland) was employed to record absorbance (OD) value at 450 nm, and the standard curve was adopted to measure LDH contents.

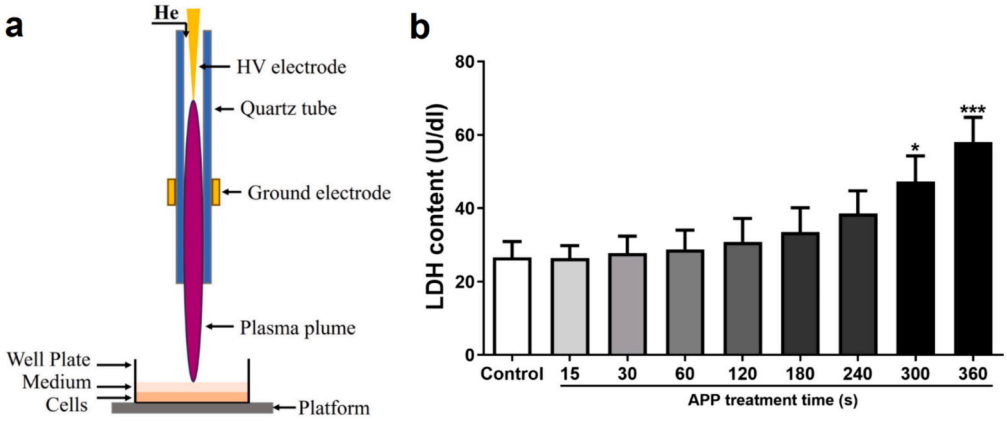

Fig. 1. The plasma device and cytotoxicity evaluation of APP treatment. (a) Schematic view of the plasma device and the experimental setup. (b) Evaluation of the cytotoxicity of the APP treatment on SH-SY5Y cells. 30–240 s APP treatment was the safe dose for the current study and was used in the following experiments. The data are expressed as the mean ± SD. $^{*}p < 0.05$, $^{**}p < 0.01$, and $^{***}p < 0.001$ compared with the control group ($n = 3$).

2.5. Cell apoptosis measurement

We collected SH-SY5Y cells from diverse groups after 18-h OGD treatment, then washed them by PBS. Annexin V-FITC and PI (KeyGen, Nanjing, China) were added for cell staining to classify apoptotic and nonapoptotic cells. The binding buffer (500 μl) was added for cell resuspension, followed by 20-min staining with 4 μl Annexin V-FITC and 3.5 μl PI solution under ambient temperature in dark. Thereafter, BD FACS Calibur cytometer with the FlowJo 7.6.1 software (Becton Dickinson, Mountain View, CA) was utilized for flow cytometry. The researcher was blinded to grouping.

2.6. NO measurement

The rat serum in each group was gathered at 24 h after MCAO. Extracellular NO levels within the medium and serum were measured with Griess reagent (Beyotime, Haimen, China) based on the manufacturer's protocol and NO levels were identified through measuring the NO_2^- content at 540 nm based on a standard curve of $NaNO_2$ (M200 Pro, Tecan, Switzerland).

In this study, 3-amino, 4-aminomethyl-2′, 7′-difluorescein, diacetate (DAF-FM DA) (Beyotime, Haimen, China) was utilized in NO content measurement within cells. After APP treatment, DAF-FM DA (10 μM) was added for 20-min of cell incubation under 37 °C. Thereafter, PBS was added for cell washing thrice, followed by measurement of fluorescence intensity at the emission and excitation wavelengths of 525 and 488 nm, respectively, with the microplate reader (M200 Pro; Tecan, Switzerland). NO level was shown as fluorescence intensity.

2.7. ROS measurement

Following the manufacturer's protocol, the extracellular and rat serum ROS contents were measured with the hydrogen peroxide Assay kit (Beyotime, Haimen, China). The culture medium (50 μl) was gathered post-APP treatment, followed by 30 min of incubation with the detection reagent under ambient temperature. The absorbance was detected at 560 nm (M200 Pro, Tecan, Switzerland). The standard curve was adopted for measuring H_2O_2 content (μM).

The DCFH-DA (Beyotime, Haimen, China) probe was used for determining ROS contents in cells. After APP treatment, DAF-FM DA (10 μM) was added for 20-min cell incubation under 37 °C. After washing with PBS thrice, the microplate reader (M200 Pro; Tecan, Switzerland) was adopted for measuring fluorescence intensity at the emission and excitation wavelengths of 525 and 488 nm, separately. ROS contents were expressed as fluorescence intensity.

2.8. Western blot analysis

Cells were subjected to 18-h OGD treatment before harvest. After on-ice lysis using cell lysis buffer (Beyotime, Haimen, China), protein content was determined with the BCA protein assay kit (Beyotime, Haimen, China). Then, 30 mg proteins/lane were separated with sodium dodecyl sulfate polyacrylamide gel electrophoresis (SDS-PAGE), and transferred on nitrocellulose membranes (Millipore, MA, USA). Thereafter, membranes were blocked using 5% defatted milk contained within TBST buffer (consisting of 150 mM NaCl, 0.1% Tween 20, as well as 20 mM Tris-HCl, pH 7.4) overnight under 4 °C. Later, primary antibodies were added for 2-h incubation, then HRP-labeled specific IgG secondary antibodies were added for another 1-h incubation under ambient temperature. Primary antibodies used included Rabbit anti-Bax (1:1000, Cat. ab32503), Rabbit anti-LC3 (1:2000, Cat. ab192890), Rabbit anti-mTOR (1:10000, Cat. ab134903), Rabbit anti-p-mTOR (1:10000, Cat. ab109268) and rabbit anti-GAPDH (1:3000, Cat. ab9485, all from Abcam), as well as rabbit anti-Bcl-2 (1:200, Cat. SC-492, Santa Cruz). Meanwhile, rabbit anti-AMPK (1:1000, Cat. 5832) and rabbit anti-p-AMPK (1:1000, Cat. 2535) were provided by Cell Signaling Technology. Signals were visualized with the enhanced chemiluminescence (ECL) kit (Pierce, USA) using the ChemiDoc system (Bio-Rad, USA). GAPDH was the control for data normalization.

2.9. Transfection of adenovirus HBAD-mRFP-GFP-LC3

Adenovirus vectors that encoded LC3 (HBAD-mRFP-GFP-LC3, HANBIO, China) were transfected into cells for autophagy flux monitoring. SH-SY5Y Cells were seeded onto the confocal plate, followed by infection with mRFP-GFP-LC3 adenovirus at 250 multiplicity of infection (MOI). After 24 h transfection, cells were subject to treatment with APP for different duration and further cultured for 6 h as mentioned above. Next, cell images were obtained using the Axio Observer Z1 fluorescence microscope (Zeiss, Germany). Image processing was performed using ImageJ software. The GFP-LC3 (green) and mRFP-LC3 (red) images were merged and yellow spot number (autophagosomes) in each cell was counted from about thirty cells of every group. The dot number/cell was acquired by dividing total dot number by nucleus number within every microscopic field.

2.10. Transmission electron microscopy (TEM)

The SH-SY5Y cells were gathered and fixed with 2.5% glutaraldehyde plus 2% paraformaldehyde for 2 h and postfixed in 1% OsO_4 under 4 °C for a 2-h period. After gradient ethanol dehydration and epoxy resin embedding, the 1-μm-thick semithin sections were first sliced using the

ultramicrotome (Leica, UC6, Wetzlar, Germany), followed by 1% toluidine blue staining. Then a representative block was selected for ultrathin sectioning. Subsequently, 70-nm-ultrathin sections were sliced, followed by double-staining using 7.3% uranyl acetate and lead citrate, as well as observation under the transmission electron microscope (H-7650, Hitachi, Japen).

2.11. Animals and MCAO surgery

Totally 44 male Sprague-Dawley rats (weight, 180–200 g) were purchased from Beijing Vital River Laboratory Animal Technology Co., Ltd. (Beijing, China). All experiments were approved by the Animal Ethics Committee of Beijing Neurosurgical Institute (approval number, 201902030). Rats were housed in a controlled environment (24 °C ± 2 °C; 3–4 animals per cage; 12-h light/dark cycle) with food and water ad libitum. After 7 days' acclimatization, rats received middle cerebral artery occlusion (MCAO) surgery when their weights reached about 250 g.

The rat model was constructed by intraluminally occluding right middle cerebral artery (MCA) according to our published method [22]. The mixture of ketamine (100 mg/kg) and xylazine (10 mg/kg) was given in every rat via intraperitoneal injection for anesthesia. Then, a silicon coated filament was inserted from external carotid artery (ECA) and internal carotid artery for MCA occlusion. At 90 min post-embolization, ischemia reperfusion was achieved through slight retrieval of the filament. Subsequently, the ECA clip was tightened, followed by suture of neck skin. Sham rats received identical surgical procedure without filament insertion. Three rats died due to subarachnoid hemorrhage (2 in the MCAO group, 1 in the MCAO+APP group).

2.12. Experimental groups and APP treatment

MCAO rats were treated with APP inhalation and were randomly divided into three groups: (1) sham operated group, $n = 11$ (4 for neurological deficit scores and TTC staining; 7 for serum H_2O_2/NO assay and histological staining); (2) MCAO group, $n = 15$ (8 for neurological deficit scores, MRI and TTC staining; 7 for serum H_2O_2/NO assay and histological staining); and (3) MCAO+APP group, n = 15 (8 for neurological deficit scores, MRI and TTC staining; 7 for serum H_2O_2/NO assay and histological staining). Rats in MCAO+APP group received 2-min APP inhalation treatment in a supine position at 60 min after MCAO surgery. At 90 min post-embolization, the filament was slightly removed to achieve reperfusion. MRI and 2, 3, 5-triphenyltetrazolium chloride (TTC) staining were performed at 24 h after MCAO.

2.13. Magnetic resonance imaging (MRI)

MRI was performed using a 7.0 T system with a 4-channel rat brain coil (Bruker, Germany) at 24 h after MCAO. Diffusion-weighted images (DWI) were acquired using the following parameters: matrix = 128 × 108, field of view = 40 × 40 mm, repetition time = 4500 ms, slice thickness = 1 mm, echo time = 35 ms, number of averages = 1, b values = 1000 s/mm^2. Quantitative maps of the apparent diffusion coefficient (ADC) were calculated based on two different b-values (0 and 1000 s/mm^2). Images were processed and lesion volumes (mm^3) were calculated using Radiant DICOM Viewer (version 2021.2) according to our previous study [23].

2.14. Neurological deficit score assessment

The improvement of neurological function was evaluated using neurological deficit scores at 24 h after MCAO according to our previous studies by one researcher blinded to rat grouping [22]. Higher scores suggest severe neurological function deficits.

2.15. TTC staining

Whole-brain samples from rats were collected at 24 h after MCAO and frozen for 1 h. Then about 2 mm-thick slices were cut along the coronal plane and stained with 2% TTC solution (Solarbio, Beijing, China) for 30 min in dark and fixed with 10% paraformaldehyde solution overnight. The healthy and infarcted tissues were stained red and white, respectively. Image-Pro Plus 6.0 was used to quantitatively analyze the infarct volume of the slices with the following formula: Infract volume (%) = ((volume of contralateral - volume of non-ischemic ipsilateral))/2 × (volume of contralateral) × 100%.

2.16. Hematoxylin-eosin (HE) staining and immunohistochemistry analysis

Rats were perfused with 4% paraformaldehyde at 24 h after MCAO. The whole brains were extracted in normal saline and then fixed in 10% paraformaldehyde, and later dehydrated and embedded in paraffin. Paraffin-embedded tissues were consecutively cut into slices with the thickness of 4 μm. Next, the slices were dewaxed by dimethylbenzene after 60 min of heating at 60 °C, and immersed in absolute, 95%, 85%, and 75% alcohol, respectively, all for the duration of 5 min. After being processed with the HE staining procedure, the slices were subject to dehydration by gradient alcohol and xylene, and finally mounted.

After repaired with sodium citrate at high temperature and pressure, the brain tissue slices were blocked with normal goat serum for 60 min and subsequently exposed to incubation in primary antibodies to 8-OHdG (sc-393,871, SANTACRUZ), at 4 °C overnight. Followed by being rinsed with PBS thrice, the slices were subject to treatment with horseradish peroxidase-conjugated secondary antibodies for 60 min under the condition of room temperature, followed by colour-reaction with a DAB visualization kit (ZLI-9017, ZSGB), and nuclear labeling with hematoxylin. Next, the slices were dehydrated, mounted and explored as the previous description.

2.17. TUNEL staining

Cell apoptosis in brain tissues was identified using the TUNEL apoptosis kit (G1501, Wuhan Servicebio Technology Co., Ltd., China) according to the relevant instructions. The brain sections were stained with appropriate TUNEL reagents and DAPI solution, followed by PBS rinsing and mounting. The slides were scanned using Pannoramic Digital Slide Scanner (Pannoramic DESK, P-MIDI, P250, 3DHISTECH Ltd.). TUNEL positive nucleus numbers were explored with ImageJ software (Version 1.8.0, National Institutes of Health). The percentage of TUNEL positive cells (%) = apoptotic nucleus number/ overall nucleus number in cerebral hemisphere×100%.

2.18. Statistical analysis

Data were expressed by mean ± standard deviation (SD) and analyzed with Prism software package (version 8.2.1). The present study compared multiple groups with one-way ANOVA and Tukey's multiple-comparison. Two groups were compared by Student's *t*-test. $p < 0.05$ was considered as statistical significance.

3. Results

3.1. Evaluation of cytotoxicity of APP treatment

The cytotoxicity of APP preconditioning was first evaluated using a LDH assay kit. SH-SY5Y cells were subject to APP treatment for diverse durations and cultured for 7 h. Then, LDH content of the culture medium was assessed to test cell damage induced by APP treatment. As presented in Fig. 1b, short-time APP treatment did not cause any significant increase in LDH release to the culture medium. With the prolonged APP

treatment, the LDH release gradually elevated, and a significant difference relative to untreated control group was found in 300 s treatment group ($P < 0.05$). Therefore, 30–240 s APP treatment was used in the following experiments.

3.2. APP treatment preconditioning increased SH-SY5Y cell autophagy

Function of APP treatment preconditioning in SH-SY5Y cells autophagy was explored. The hallmark protein of autophagy LC3-II was determined by western-blot. Based on Fig. 2a and b, LC3-II expression significantly increased with the APP treatment time. Meanwhile, we also detected the autophagy-related proteins and found that the expression of ATG 7 and ATG 12 elevated with the APP treatment, indicating that cell autophagy was activated by the APP treatment dose-dependently.

Additionally, the cell autophagy was also confirmed by tandem adenovirus mRFP-GFP-LC3 transfection for monitoring the autophagic flux. Yellow (mRFP and GFP) and red (only mRFP) signals were used to identify autophagosomes and autolysosomes, respectively. The number of autophagosomes and autolysosomes (LC3-labeled yellow and red puncta, respectively) elevates with an increase in autophagic flow. In our present study, relative to untreated control group, both autophagosomes (yellow) and autolysosomes (red) within SH-SY5Y cells were

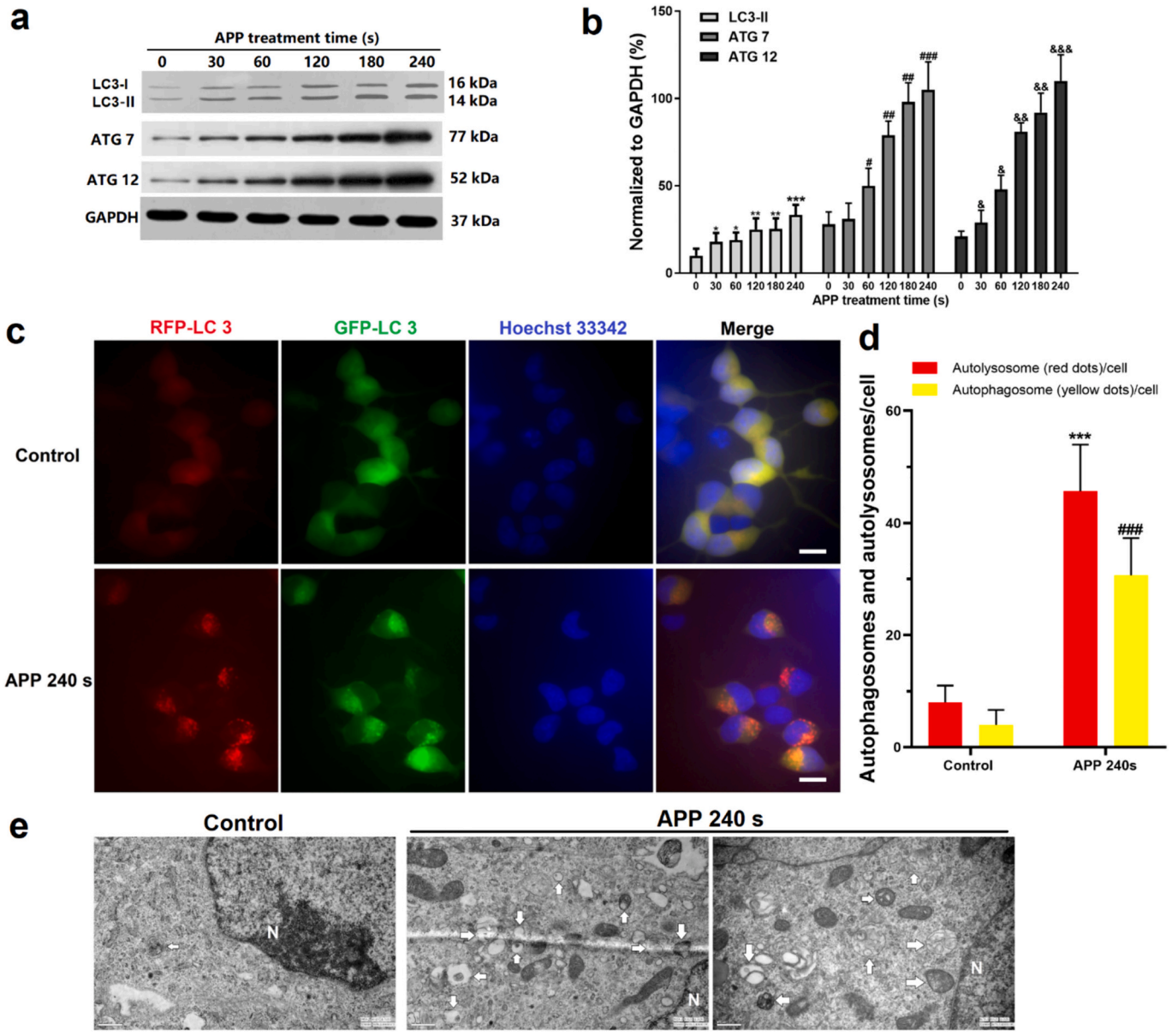

Fig. 2. APP treatment preconditioning promoted SH-SY5Y cells autophagy. (a) The expression of LC3, ATG 7 and ATG 12 was measured using western blotting. (b) Each protein was quantitatively explored in each group. The error bars indicate the mean ± SD. $*p < 0.05$, $**p < 0.01$, and $***p < 0.001$ compared with the untreated control group of LC3-II. $\#p < 0.05$ and $\#\#p < 0.01$ in relative to the untreated control group of ATG 7. $\&p < 0.05$, $\&\&p < 0.01$, and $\&\&\&p < 0.001$ in relative to the untreated control group of ATG 12 (n = 3). (c) Representative images of LC3 staining in SH-SY5Y cells infected with mRFP-GFP-LC3 in each group were indicated. The autophagosomes were shown by yellow puncta and autolysosomes were shown by red puncta. Scale bars show 10 μm. (d) Quantification of the autolysosomes and autophagosomes was counted and calculated using Image Pro. The findings were acquired from three independent experiments with at least 100 cells explored. The data are expressed as the mean ± SD. $***p < 0.001$ compared with control group of autolysosomes. $\#\#\#p < 0.001$ in relative to control group of autophagosomes. (e) Representative images of autophagic vacuole formation in SH-SY5Y cells in each group were shown. N represented nucleus. The arrows labeled autophagosomes (scale bar 500 nm, original magnification 25,000×). (For interpretation of the references to colour in this figure legend, the reader is referred to the web version of this article.)

clearly observed in the APP treatment group, indicating the increased autophagy flux level by the APP treatment (Fig. 2c-d).

Furthermore, as the golden standard autophagy detection, we also employed TEM microscopy to observe the autophagosomes. The formation of double-membrane autophagosomes, which contained cytoplasmic material and/or organelles for later breakdown, is the morphological hallmark of general autophagy. Autophagosomes will fuse with lysosomes to generate mature autolysosomes, which could fuse into one membrane structure. As indicated by Fig. 2(e), autophagosome number of APP treatment group apparently increased, indicating that APP treatment preconditioning increased SH-SY5Y cell autophagy.

3.3. APP preconditioning reduced OGD induced SH-SY5Y cell apoptosis

Different duration of OGD induced SH-SY5Y cell injuries were first evaluated to optimize the suitable OGD treatment time. As shown in Fig. 3a, SH-SY5Y cell viability gradually decreased as OGD treatment duration increased and decreased by about 50% when the OGD treatment time reached 18 h. The following cell injury experiments used an OGD damage time of 18 h.

The effect of the APP preconditioning on OGD induced SH-SY5Y cell death was further revealed. As shown in Fig. 3b, APP preconditioning reduced LDH release resulted from OGD injuries, indicating the cytoprotective effect of the APP treatment. Furthermore, cell apoptotic rate in each group was measured using AnnexinV-FITC and PI double-staining assay and was analyzed by flow cytometry (Fig. 3c and d). Compared with control group, OGD treatment significantly lowered the percentage of living cells, which was reversed by the APP treatment in a dose dependent manner.

Cell apoptosis-related proteins were analyzed. As displayed in Fig. 3e-3f, in comparison with control group, OGD dramatically reduced the antiapoptotic protein Bcl-2 level and promoted the proapoptotic protein Bax level. Meanwhile, the cleaved caspase-3, the executor of cell apoptosis which is an activated form of caspase-3, was also down-regulated by the OGD injuries. APP preconditioning significantly diminished the changes induced by OGD dose-dependently, indicating the cytoprotective impact of the APP preconditioning on OGD induced cell apoptosis.

Furthermore, the morphological changes of SH-SY5Y cells were further found by Calcein-AM staining. Calcein-AM rapidly entered viable cells and converted to calcein by intracellular esterases to produce green fluorescence. According to Fig. 3g, SH-SY5Y cells in OGD group became smaller, and the calcein fluorescence could not be observed in some injured cells. With the increased APP treatment, the cell morphology was improved and the calcein-negative cell number was significantly lowered.

3.4. APP treatment induced SH-SY5Y cell autophagy contributed to cytoprotection against OGD injuries

The role of the plasma-induced autophagy on the cytoprotective effect against OGD injuries was further studied. SH-SY5Y cells were pretreated by 3-Methyladenine (3-MA) followed by APP preconditioning and OGD injury. Autophagy related proteins LC3, ATG 7, ATG 12, Bcl-2 and Bax were tested. Results in Fig. 4a-4f, 3-MA showed that pretreatment significantly weakened the APP induced upregulation of LC3-II, ATG 7 and ATG 12 in SH-SY5Y cells. However, the inhibitory effect of 3-MA on APP preconditioning did not significantly induce upregulation of Bcl-2. Then, cells were exposed to the OGD conditions to evaluate the functions of autophagy in the cytoprotection of APP preconditioning. As shown in Fig. 4g, 3-MA abolished protection of APP on OGD-mediated SH-SY5Y cell injuries, indicating the cytoprotective effect of the APP preconditioning was achieved by the autophagy activation.

3.5. APP preconditioning induced ROS/RNS elevation

The biomedical function of the plasma is mainly based on its production of ROS and RNS. To further investigate the mechanism of APP-induced autophagy in SH-SY5Y cells to reduce OGD damage, we firstly examined the active species generated by the plasma using optical emission spectroscopy. Fig. 5a displays the optical emission spectrum (OES) of APPJ. The emission lines of OH (309 nm), N_2 (315.9 nm), N^{2+} (391.4 nm), He (706.5 nm), O (777.2 nm) and other species could be clearly observed in the spectrum and are marked in this figure, indicating that the active plasma species mainly contained oxygen and nitrogen related particles.

The plasma induced extracellular and intracellular ROS/RNS changes were further monitored. We examined the changes in ROS and RNS immediately and 7 h after plasma treatment. Extracellular ROS were indicated by the H_2O_2 content, extracellular and intracellular RNS were indicated by the NO production. As shown in Fig. 5b and e, APP treatment was able to cause an immediate rise in intracellular and extracellular ROS and NO, while the amount of ROS was significantly higher than the amount of NO. We further examined the changes in intracellular ROS and NO contents after 7 h, and the results showed that after 7 h of plasma treatment, the generation of both intracellular ROS and NO significant decreased, and the final contents were nearly the same (Fig. 5f-5g).

Since OGD induced cell apoptosis was accompanied with the increased intracellular ROS and RNS, the endogenous ROS and RNS levels in SH-SY5Y cells of each group were further detected using the fluorescent probes. Results showed that, OGD for 18 h significantly increased the intracellular ROS and RNS contents, which could be reversed by APP preconditioning in a dose-dependent manner (Fig. 5h-5i).

3.6. Scavengers of ROS and RNS abolished SH-SY5Y autophagy and the cytoprotective effect of APP preconditioning

The ROS scavenger NAC and RNS scavenger carboxy-PTIO were used to pretreat SH-SY5Y cells to further explore the impact of ROS/RNS produced by APP on autophagy and the cytoprotective effect of APP preconditioning. As shown in Fig. 6a-6f, NAC alone or combined with carboxy-PTIO obviously reduced the expression of LC3-II, ATG 7 and ATG 12. Meanwhile, although the effect of NAC alone was not significant, it significantly reduced APP-induced upregulation of Bcl-2 expression when combined with PTIO. These results indicated that the autophagy was inhibited by the ROS scavenger as well as the combination of NAC and carboxy-PTIO. Although carboxy-PTIO alone could inhibit LC3-II, ATG 7 and ATG 12 expression to some extent, the effect was much less pronounced than that of NAC, and it was not statistically significant relative to control group. Additionally, based on these findings, carboxy-PTIO slightly reduced the cytoprotective effect against OGD injuries produced by the APP preconditioning, and the results were not statistically significant. In contrast, NAC alone or combined with carboxy-PTIO markedly abolished the cytoprotective effect of APP preconditioning. These findings suggestthat ROS have a dominant effect on the cytoprotection of APP preconditioning against OGD injuries.

3.7. Cytoprotective effect of APP preconditioning was mediated by the ROS/AMPK/mTOR pathway

As a vital downstream signaling pathway of ROS for regulating autophagy, AMPK/mTOR pathway was further investigated to study the mechanisms of the cytoprotective effect of the APP preconditioning. As shown in Fig. 7a and b, the ratio of p-AMPK/t-AMPK markedly increased while that of p-mTOR/mTOR decreased with the prolonged APP treatment time. Consequently, AMPK/mTOR pathway was activated by the APP preconditioning. The selective AMPK inhibitor CC was used to pretreat SH-SY5Y cells for 1 h before APP treatment to check the impact

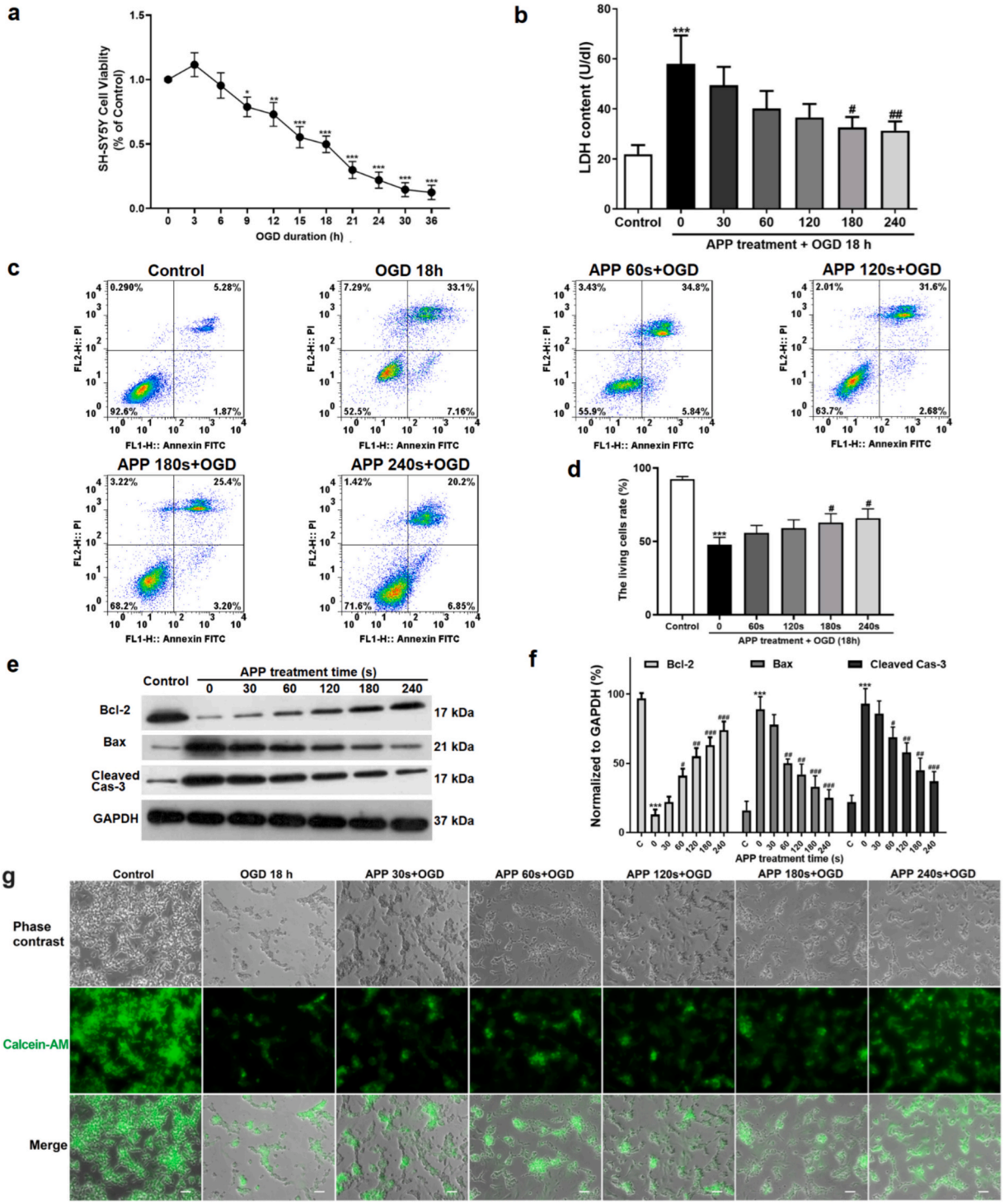

Fig. 3. Cytoprotective effects of the APP preconditioning on OGD induced SY-SY5Y cells apoptosis were detected. (a) Impact of different OGD duration on SH-SY5Y cell injuries were evaluated to optimize the suitable OGD treatment time. 18 h OGD induced about 50% cell viability decrease and was selected for the following experiments. $*p < 0.05$, $**p < 0.01$, and $***p < 0.001$ compared with the control group ($n = 3$). (b) APP preconditioning reduced LDH release caused by OGD injuries in a dose dependent manner. The data are indicated as the mean ± SD. $***p < 0.001$ compared with the control group; $\#p < 0.05$ and $\#\#p < 0.01$ in relative to the OGD group ($n = 3$). (c) Representative images of flow cytometry analysis of apoptotic SH-SY5Y cells in each group. (d) Quantification of the proportion of living cells in each group. $***p < 0.001$ in relative to the control group; $\#p < 0.05$ in relative to the OGD group ($n = 3$). (e) The expression of apoptotic related proteins Bcl-2, Bax and cleaved-caspase 3 in each group were detected by western blotting. (f) Each protein was quantitatively analyzed in each group. The error bars indicate the mean ± SD. $***p < 0.001$ compared with the untreated control group. $\#p < 0.05$, $\#\#p < 0.01$ and $\#\#\#p < 0.001$ compared with the OGD group ($n = 3$). (g) The morphological changes of SH-SY5Y cells in each group further identified by Calcein-AM staining and observed by contrast light microscopy and calcein-AM fluorescence imaging. Scale bars show 50 μm.

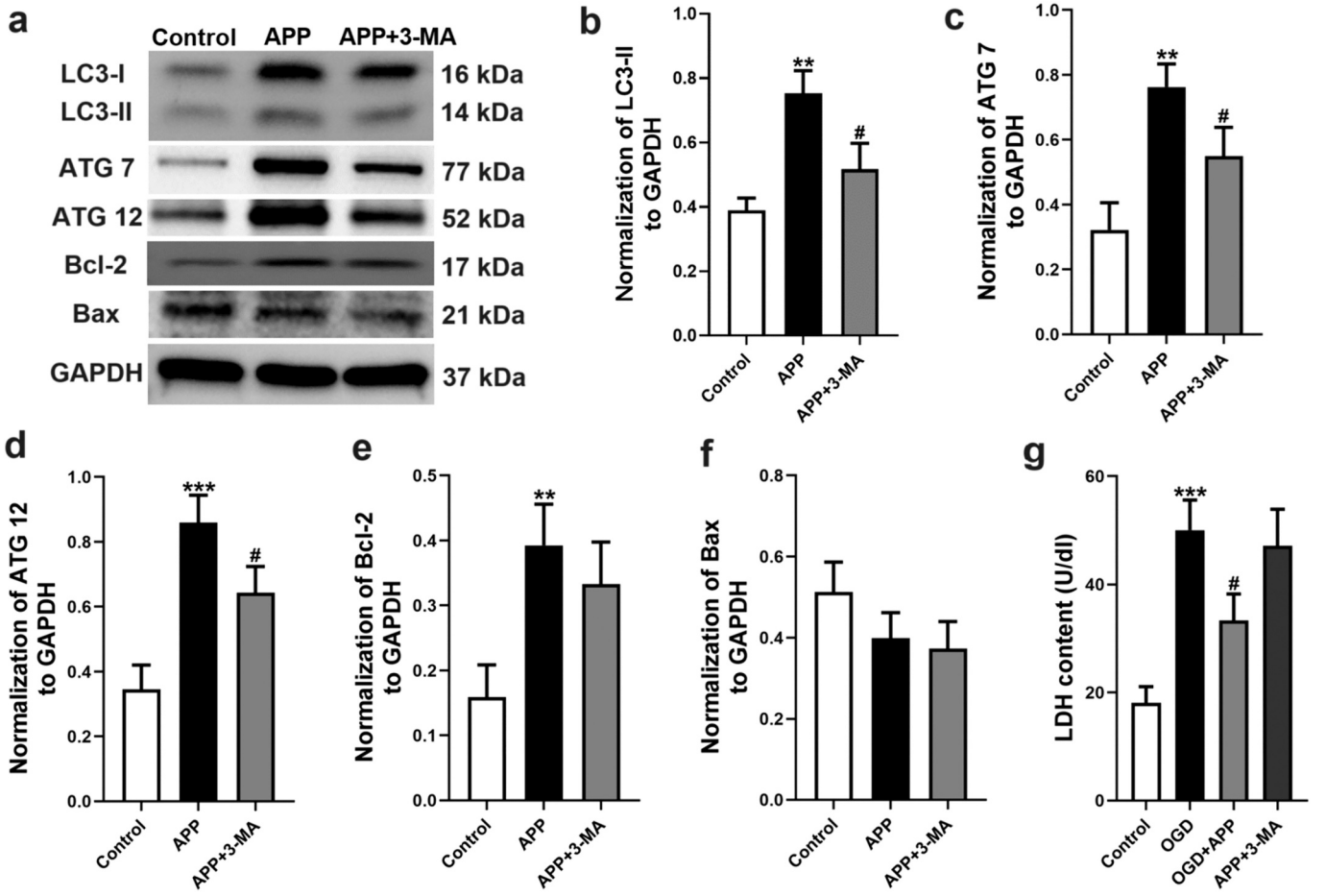

Fig. 4. Effect of APP preconditioning induced autophagy on the cytoprotective effect against OGD injuries. (a) The expression of the autophagy related proteins in the APP treatment and autophagy inhibitor 3-MA pretreatment groups were detected using western blotting. (b-f) The protein levels of LC3-II, ATG7, ATG 12, Bcl-2 and Bax in each group were statistically analyzed. The error bars indicate the mean ± SD. $^{**}p < 0.01$ compared with the untreated control group. $\#p < 0.05$ compared with the APP treatment group ($n = 3$). (g) Cell viability was detected by the measurement of LDH release in the medium. 3-MA abolished the protective effect of APP on OGD induced SH-SY5Y cell injuries. The error bars indicate the mean ± SD. $^{**}p < 0.01$ and $^{***}p < 0.001$ compared with the untreated control group. $\#p < 0.05$ compared with the OGD group (n = 3).

of AMPK/mTOR pathway on the cytoprotective effect of APP preconditioning against OGD injuries. As shown in Fig. 7c-7e, CC reduced the LC3-II level of SH-SY5Y cells and abolished the cytoprotective effect of the APP preconditioning against OGD injuries. In addition, it was found that, similar to the 3-MA and NAC, CC reduced p-AMPK/t-AMPK ratio and increased p-mTOR/mTOR ratio which was induced by the APP preconditioning (Fig. 7f-7g). Our results indicate that APP preconditioning can protect SH-SY5Y cells from OGD injuries by activating autophagy and ROS/AMPK/mTOR pathway.

3.8. APP inhalation reduces cerebral infarct volume in MCAO rats

The cytoprotective effect of APP was preliminary confirmed in MCAO rats. The photograph of the plasma plume and application for the rats is shown in Fig. 8a. Rats could inhale the plasma by nasal directly. Fig. 8b shows the experiment procedure. Rats in MCAO+APP group received 2-min APP inhalation treatment in a supine position at 60 min after MCAO surgery. Effect of APP inhalation on ischemic stroke rat model was evaluated at 24 h after MCAO. The neurological function was first assessed using neurological deficit scores, and results demonstrated that MCAO significantly caused neurological function impairment which could be improved by the APP inhalation (Fig. 8c). The low signal (dark) zone in ADC images of MRI defined the ischemic lesions. As shown in Fig. 8d-8e, relative to the MCAO group, APP inhalation significantly reduced ADC-defined ischemic lesions from 304.5 ± 41.93 mm^3 to 156.8 ± 33.17 mm^3 ($p < 0.001$). Furthermore, the brain infarction was also evaluated using TTC staining. It was demonstrated that, APP inhalation significantly reduced the infarction volume of MCAO rats from 36.44 ± 3.79% to 18.13 ± 4.38% (Fig. 9f-9 g, $p < 0.001$). In Fig. 8h-8i, APP inhalation significantly reduced the serum H_2O_2 and NO concentrations induced by ischemic brain injuries. Then, the histological staining was performed to observe the morphology and pathological changes of the brain tissues in each group. The magnified view indicated by the boxes was selected based on MRI results which was boundary of the lesion regions. As shown in Fig. 8j, most cells were arranged disorderly, whereas the loose tissue structure and the pyknotic nuclei could be observed, which were attenuated by the APPJ inhalation. Meanwhile, TUNEL staining indicated that APP treatment reduced the MCAO caused cell apoptosis in brain tissues (Fig. 8k-8i). Furthermore, the oxidative stress levels of brain tissues were accessed by 8-OHdG IHC staining. As shown in Fig. 8m- 8n, 8-OHdG expression in MCAO group was significantly increased compared with the sham control, which could be mitigated by APP inhalation treatment.

4. Discussion

Our previous studies have shown the neuroprotective effect of APP treatment both in vivo and in vitro [19,20,22,23], and are consistent with other studies [21,24]. However, the detailed biological mechanisms were still unclear. In our current work, we discovered that APP

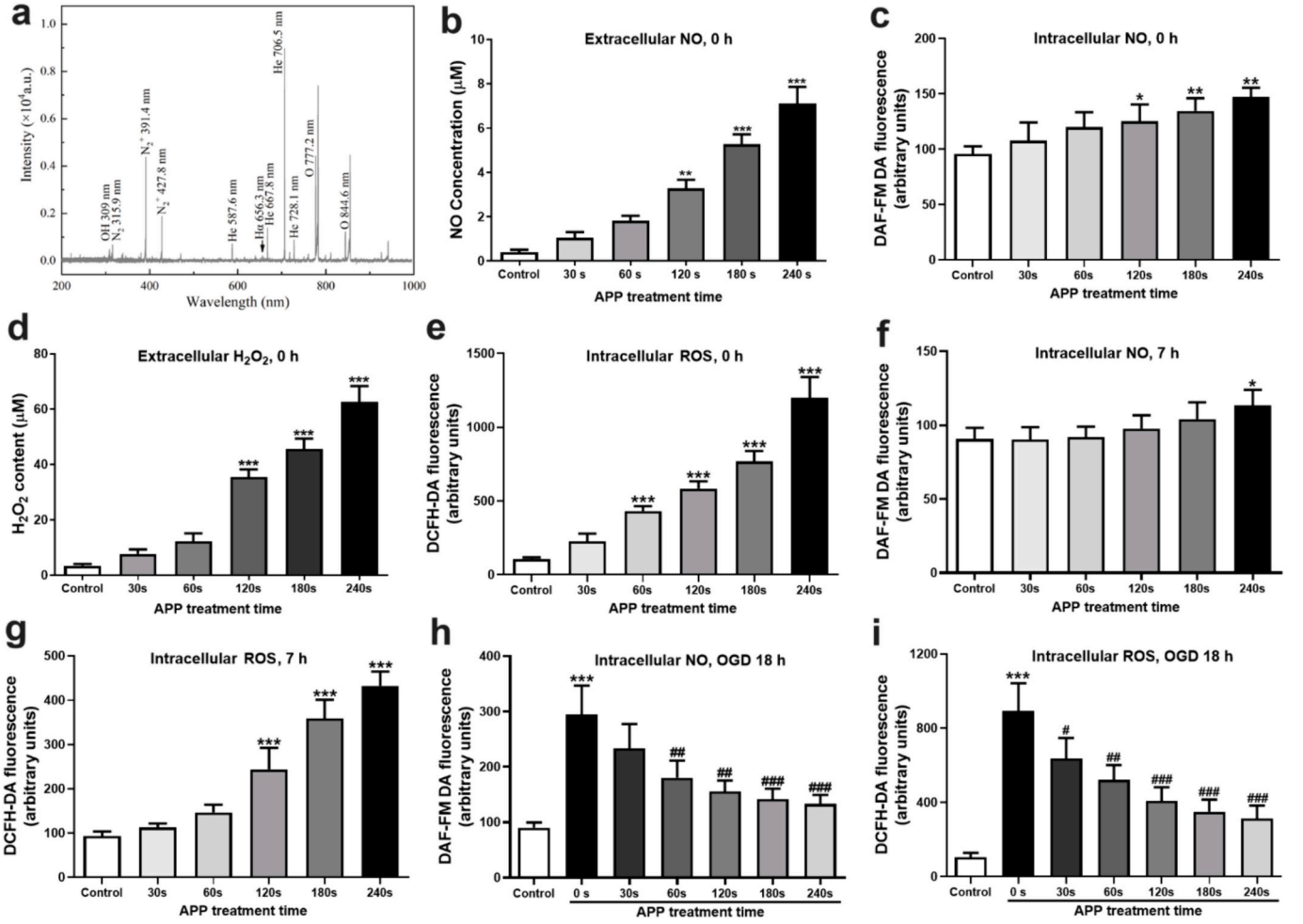

Fig. 5. Higher ROS/RNS levels induced by the APP preconditioning. (a) Representative OES spectra of the APP. The emission lines of OH (309 nm), N_2 (315.9 nm), N^{2+} (391.4 nm), He (706.5 nm), O (777.2 nm) were marked in this figure. (b) and (c) The extracellular and intracellular NO was measured immediately (0 h) after the APP treatment using Griess reagent and DAF-FM DA staining respectively. (d) and (e) The extracellular and intracellular ROS was measured immediately (0 h) after APP treatment using hydrogen peroxide Assay kit and DCFH-DA staining respectively. (f) and (g) The intracellular NO and ROS contents at 7 h after APP treatment were measured using DAF-FM DA and DCFH-DA staining respectively. (h-i) The intracellular NO and ROS contents of each group at 18 h after OGD were measured using DAF-FM DA and DCFH-DA staining respectively. The error bars indicate the mean ± SD. $^*p < 0.05$, $^{**}p < 0.01$, and $^{***}p < 0.001$ compared with the control group (n = 3).

treatment preconditioning could increase the SH-SY5Y cells autophagy and decrease cell apoptosis caused by OGD in a dose-dependent manner. Furthermore, the protective effect of APP treatment was also confirmed in the rat MCAO model and results showed that inhalation of APP via nasal by rat during MCAO process could reduce the brain infarct volume and reperfusion injuries. It was also found that the autophagy inhibitor 3-MA abolished the cytoprotective effect of the APP treatment conditioning, suggesting that the autophagy triggered by the APP preconditioning directly contributed to its cytoprotective functions against OGD injuries. The relationship between the APP treatment and the autophagy was established and the findings demonstrated that APP treatment notably elevated the extracellular and intracellular ROS/RNS productions. The ROS scavenger NAC as well as the combination of NAC and carboxy-PTIO abolished the APP preconditioning induced SH-SY5Y autophagy and the cytoprotection, while the NO scavenger alone did not, suggesting that ROS generated by APP preconditioning played a dominant role in the cytoprotective effect against OGD injuries. Furthermore, the biological mechanism was studied. It was found that the ROS downstream AMPK/mTOR pathway was activated by APP preconditioning in a dose-dependent manner. The AMPK inhibitor CC, the ROS scavenger NAC and autophagy inhibitor 3-MA could suppress the AMPK/mTOR pathway and abolish the cytoprotective effect of APP preconditioning against OGD injuries, suggesting that APP preconditioning could protect SH-SY5Y cells from OGD injuries by activating autophagy and ROS/AMPK/mTOR pathway.

The ROS and RNS produced by plasma play a central role in their biomedical applications. Most studies focus on the application of plasma on sterilization and tumor suppression based on the oxidative/nitrative stress produced by plasma [18]. However, both ROS and RNS in appropriate low concentration also play crucial physiological roles in signal transduction, cell proliferation, cytoprotection and other processes [17]. On the other hand, the composition and relative content of reactive species are influenced by the plasma generation and treatment conditions, which can be optimized for specific biomedical applications. In the present study, the plasma generation and treatment parameters were “milder” compared with that of previous studies, and it may be much suitable for the plasma use to avoid the excessive treatment induced tissue injuries. Abundant studies have shown that plasma exposure can induce cell death through activating autophagy in cancer cells, based on its generation of ROS/RNS and its interaction with liquid and tissues or cells [25], which requires longer plasma treatment time [26], higher discharge voltage [27] or longer incubation time after plasma treatment [28] to guarantee the sufficient amount of ROS/RNS interacting with cancer cells. The current study applied shorter APP

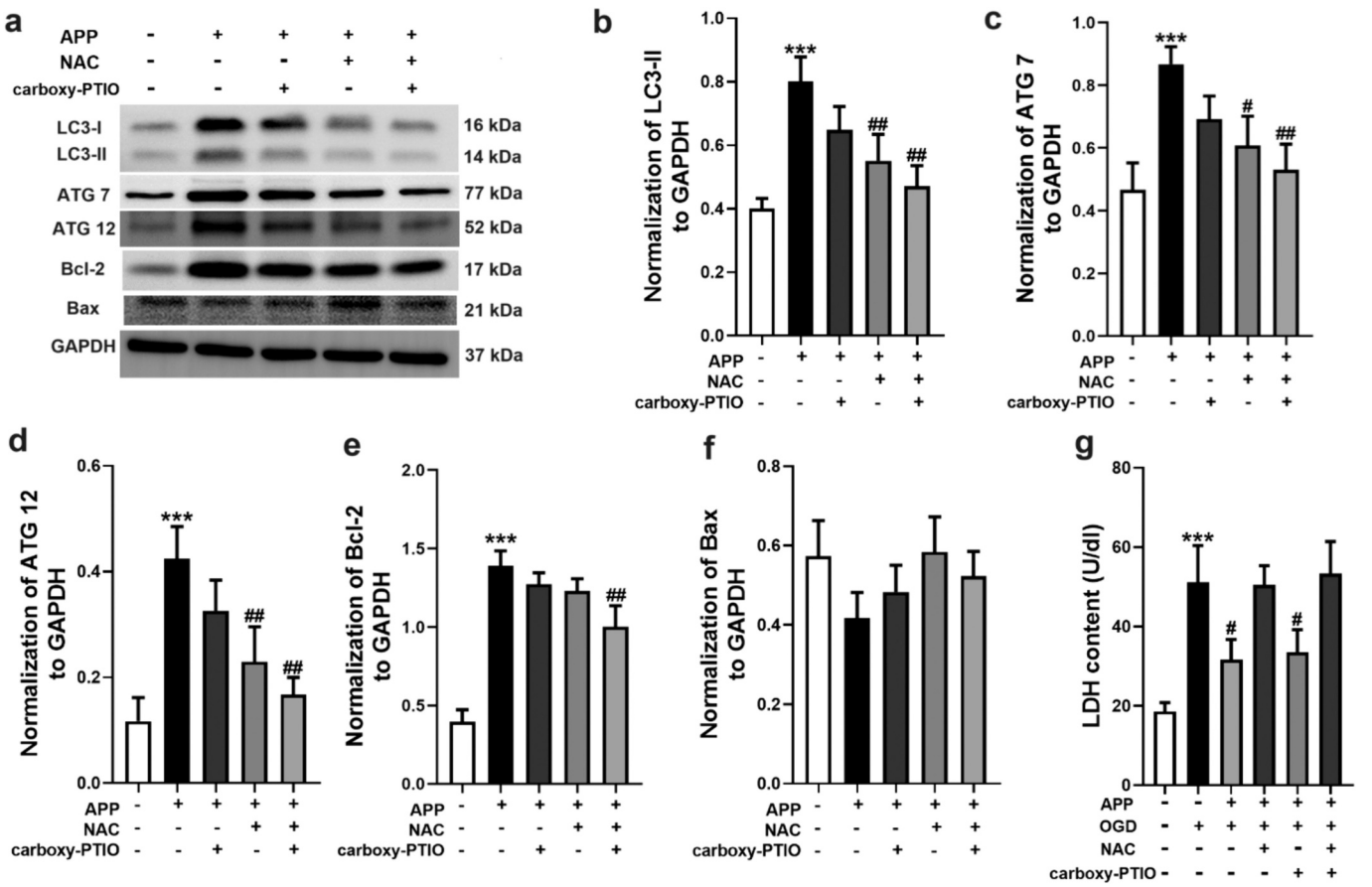

Fig. 6. Effects of the ROS and RNS scavenger on SH-SY5Y autophagy and the cytoprotective impact of the APP preconditioning. (a) The expression of the autophagy related proteins in the APP treatment, ROS scavenger NAC and RNS scavenger carboxy-PTIO pretreatment groups were detected using western blotting. (b-f) The protein levels of LC3-II, ATG7, ATG 12, Bcl-2 and Bax in each group were statistically analyzed. The error bars indicate the mean ± SD. $***p < 0.001$ compared with the untreated control group. $\#\#p < 0.01$ compared with the APP treatment group (n = 3). (g) Cell viability was detected by the measurement of LDH release in the medium. NAC alone or combined with carboxy-PTIO abolished the protective effect of APP on OGD induced SH-SY5Y cell injuries. The error bars indicate the mean ± SD. $***p < 0.001$ compared with the untreated control group. $\#p < 0.05$ and $\#\#p < 0.01$ compared with the OGD group (n = 3).

treatment time and shorter incubation time in SH-SY5Y cell and MCAO rat treatment, and the results showed the protective effects of APP treatment in vitro and in vivo on the related ischemic brain injuries.

It has been extensively accepted that autophagy is a self-protecting cellular catabolic pathway, and is central to the maintenance of cellular homeostasis in both physiological and pathological situations [29]. In the central nervous system, it is generally shown that autophagy produces protective impacts both in an OGD-treated neuronal model and cerebral ischemia model, by hindering neuronal apoptosis via multiple signal pathways [30]. In this work, effects of APP preconditioning on SH-SY5Y cell autophagy and cytoprotective against OGD injuries were first validated. The autophagy related proteins LC3, ATG 7 and ATG 12 were notably up-regulated by APP preconditioning. Meanwhile, OGD significantly decreased the antiapoptotic protein Bcl-2 and increased proapoptotic protein Bax expression, accompanied by the increased apoptotic rate of SH-SY5Y cells, which could be reversed by the APP preconditioning. Additionally, Bcl-2 and Bax also make vital impacts on the crosstalk between autophagy and apoptosis [31]. Bcl-2 can interact with Beclin-1 protein and form the Bcl-2/Beclin-1 complex via the BH3 domain of Beclin-1, which can inhibit the autophagic cell death [32]. Bax-induced autophagy has also been shown to contribute to the apoptosis in response to mitochondrial stress [31]. In order to further evaluate the correlation of APP induced autophagy and cytoprotection, the autophagy inhibitor 3-MA was employed to pretreat cells before APP treatment. The obtained findings suggested that, with the treatment of 3-MA, the LC3-II, ATG 7 and ATG 12 expressions were significantly reduced and the neuro-protective effect of APP preconditioning was abolished, suggesting that the cytoprotective effect of APP preconditioning was achieved by the autophagy activation. Although APP increased the Bcl-2 expression, 3-MA had no significant effect on Bcl-2 expression. Meanwhile, Bax expression was not significantly affected by both APP preconditioning or the inhibitors of the signal factors, suggesting that the primary roles of Bcl-2 and Bax in APP preconditioning and protection of OGD-injured neuronal cells were as anti-apoptotic and pro-apoptotic proteins rather than the autophagy regulators.

The free radical functions induced by APP treatment were then studied. As an important reactive species of plasma irradiation, NO has been proved to make a crucial role of plasma in sterilization, cancer therapy and cytoprotection, depending on the treatment time and amount [17]. Low-dose NO can not only act as a vasodilator to increase blood flow to tissues and relieve ischemic injuries, but is also a signaling molecule that regulats cell proliferation, endogenous defense system, immune response and cytoprotection [33]. It has shown that NO itself can directly induce autophagy, which contributes to reduce cell apoptosis in dental pulp [34] and kidney [35], and exert hepatoprotective effects [36]. Our previous study found that the neuroprotective effect of plasma treatment in vitro was regulated by RNS and NO/cGMP/PKG signaling pathway in certain plasma generation and treatment parameters [19]. It is also noticed that, in the presence of ROS, cGMP can react with NO to produce 8-nitro-cGMP, which can trigger S-guanylation of cell surface proteins and further induce Lys63-

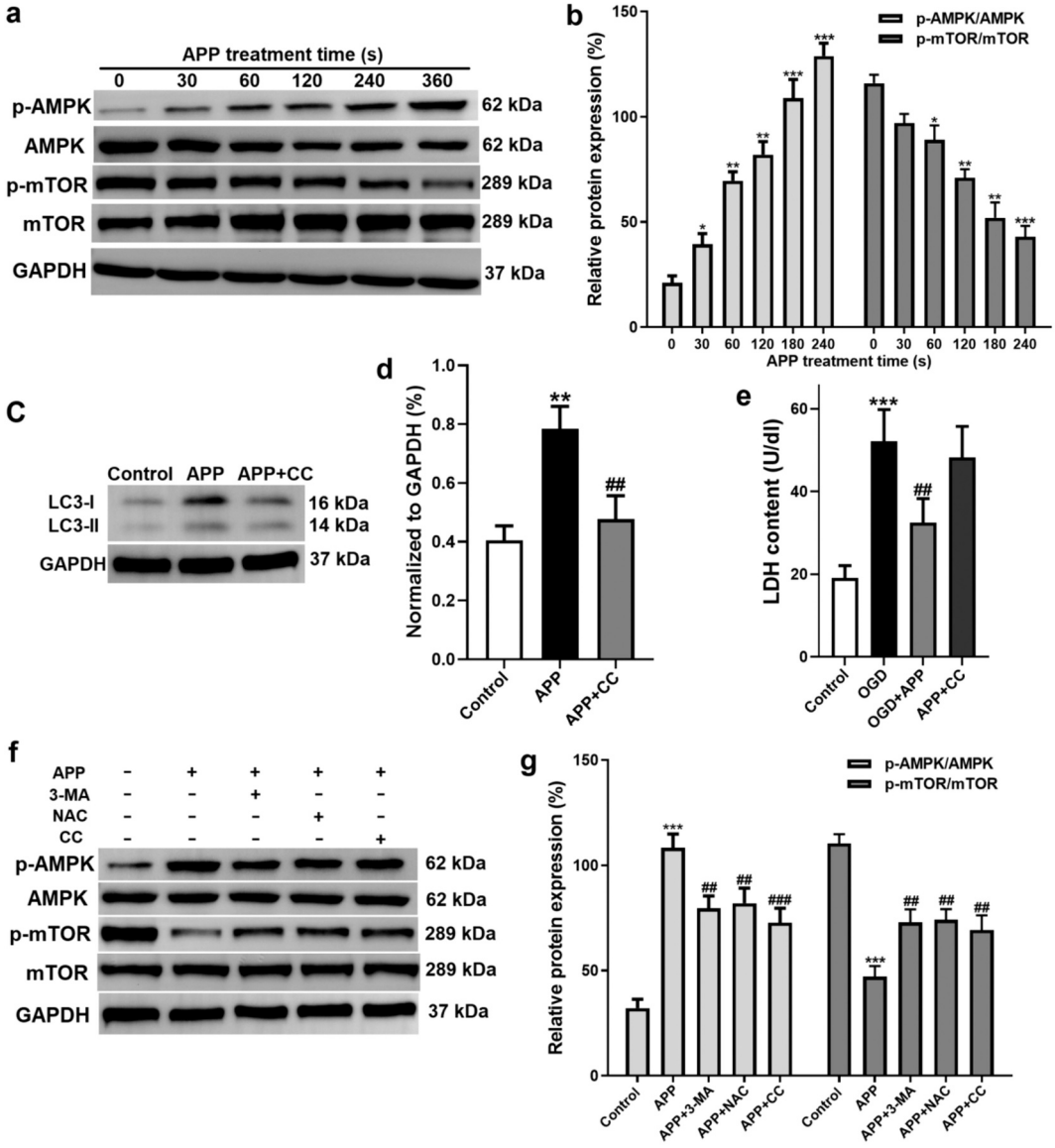

Fig. 7. Effect of the AMPK/mTOR pathway on the cytoprotective impact of the APP preconditioning against OGD injuries. (a) Effect of APP treatment on AMPK/mTOR pathway was detected using western blotting. (b) Quantitative data was analyzed for p-AMPK/AMPK and p-mTOR/mTOR. The error bars indicate the mean ± SD. $*p < 0.05$, $**p < 0.01$, and $***p < 0.001$ compared with the untreated control group (n = 3). (c) The LC3-II expression change in the APP treatment and AMPK inhibitor CC pretreatment groups were detected using western blotting. (d) Quantitative data was analyzed for LC3-II/GAPDH. The error bars indicate the mean ± SD. $**p < 0.01$ in relative to the untreated control group. $\#\#p < 0.01$ in relative to the APP treatment group (n = 3). (e) Cell viability in each group was detected by the measurement of LDH release in the medium. CC abolished the protective effect of APP on OGD induced SH-SY5Y cell injuries. The error bars indicate the mean ± SD. $***p < 0.001$ compared with the untreated control group. $\#\#p < 0.01$ compared with the OGD group (n = 3). (f) Effect of APP treatment, 3-MA, NAC and CC on AMPK/mTOR pathway was evaluated using western blotting. (g) Quantitative data was analyzed for p-AMPK/AMPK and p-mTOR/mTOR of each group. APP treatment elevated p-AMPK/AMPK ratio and reduced p-mTOR/mTOR ratio, which could be reversed by 3-MA, NAC and CC. The error bars indicate the mean ± SD. $***p < 0.001$ compared with the untreated control group. $\#\#p < 0.01$ and $\#\#\#p < 0.001$ compared with the APP treatment group (n = 3).

linked ubiquitination to facilitate its recognition by the autophagic machinery [37]. Meanwhile, exogenous 8-Nitro-cGMP also induces non cytotoxic autophagy without involving mTOR [38]. Furthermore, in the fibroblasts, it has been found that NO and downstream cyclic guanosine monophosphate (cGMP) can activate the cytoprotective autophagy, lysosomal degradation pathway and induce the selective autophagy receptor p62/SQSTM1 expression, which is a hallmark of upregulation of autophagy activity [39]. In the current study, we first detected the main reactive species in the plasma using OES, the N related and O related spectrum could be found and O related spectrum was significantly higher than that of N. It was further confirmed by the extracellular ROS and NO detection that, APP preconditioning induced more ROS productions compared with NO at 0 h after treatment. Therefore, the scavenger of NO alone has no effect on SH-SY5Y cell autophagy and OGD induced injuries.

ROS is another important class of reactive species produced by plasma. Although most studies agreed that ROS-induced oxidative stress is harmful to cells and tissues, ROS is also a vital signaling molecule in human body that maintains physiological functions and homeostasis via a series of intracellular signaling pathways [40]. ROS at low physiological concentrations are directly involved in the immune response, defense and inflammation, which is closely dependent on the timing and amount of ROS production [41]. Studies have indicated that appropriate low-dose ROS preconditioning can protect neuronal cells against multiple injuries [42,43]. Furthermore, preconditioning by an in situ administration of hydrogen peroxide can reduce the infarct size of

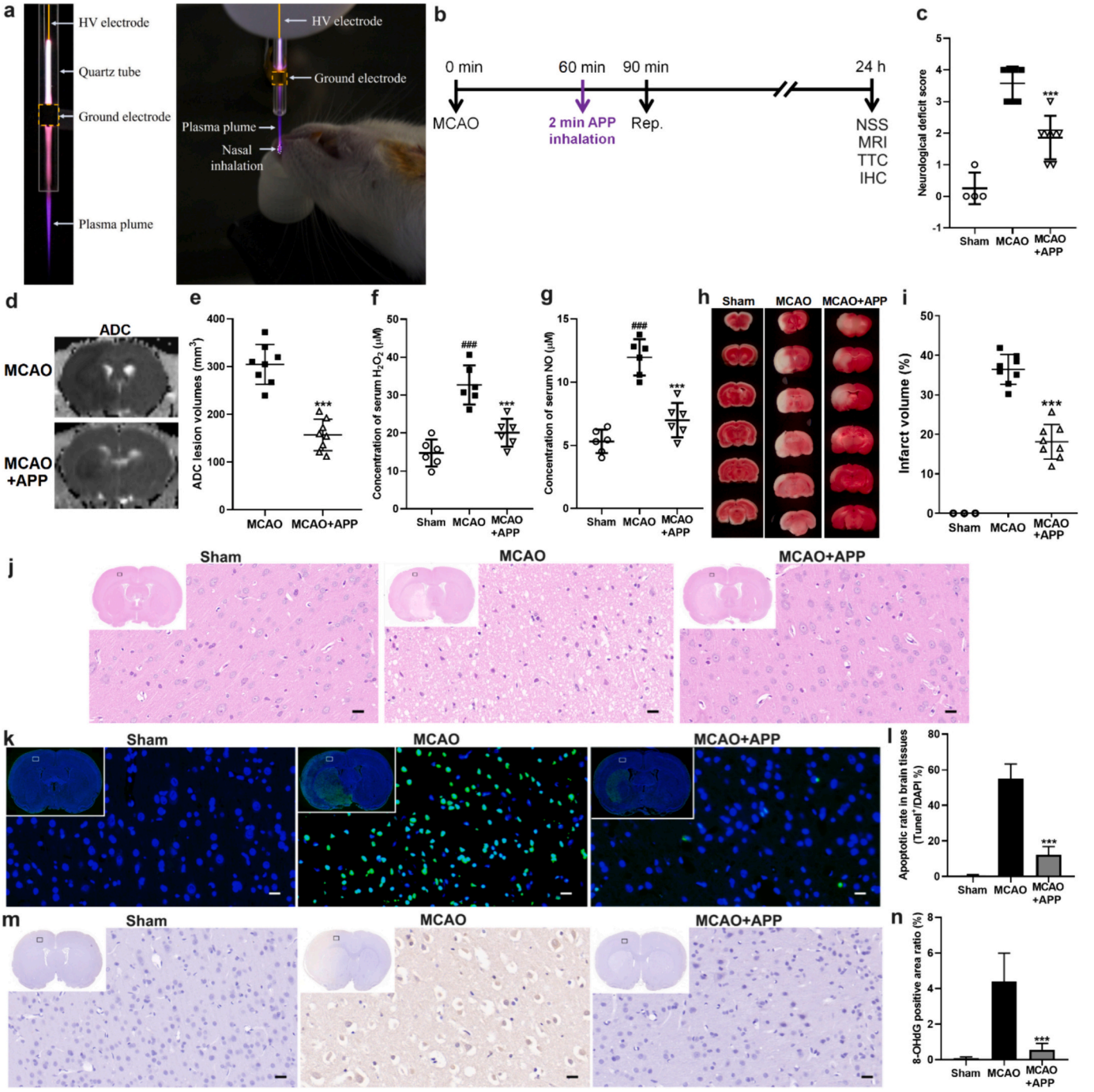

Fig. 8. Therapeutic effect of APP treatment in the MCAO rats was confirmed. (a) The photograph of the plasma plume and application for the rats. (b) The experimental procedure of the in vivo studies. (c) Effect of APP inhalation on neurological severity scores in each group. Each point indicates raw data for respective rats. (d) Representative ADC images of different groups at 24 h after MCAO. (e) ADC-defined ischemic lesion volume in each group was measured at 24 h post MCAO. Each point indicates raw data for respective rats. ***$p < 0.001$ compared with the MCAO group. (f) Representative images of TTC-stained sections from each group, where the living tissues were red, whereas infarcted tissues were white. (g) TTC-defined infarct size in each group was measured. Each point indicates raw data for respective rats. ***$p < 0.001$ compared with the MCAO group. (h-i) The concentrations of serum H_2O_2 and NO were measured at 24 h after MCAO. Each point indicates raw data for respective rats. ###$p < 0.001$ compared with the sham group. ***$p < 0.001$ compared with the MCAO group. (j) The morphology and pathological changes of the brain tissues in each group were observed by HE staining. The magnified view indicated by the boxes was selected which was boundary of the lesion regions in MCAO group. Scale bars show 20 μm. (k) Cell apoptosis in brain tissues of each group was detected by TUNEL staining. The magnified view indicated by the boxes was selected which was boundary of the lesion regions in MCAO group. Scale bars show 20 μm. (l) Quantitation of apoptotic rate in brain tissues ($n = 7$/group). ***$p < 0.001$ compared with the MCAO group. (m) Oxidative stress levels of brain tissues were accessed by 8-OHdG IHC staining. The magnified view indicated by the boxes was selected which was boundary of the lesion regions in MCAO group. Scale bars show 20 μm. (n) Statistical analysis of 8-OHdG level in brain tissues from each group (n = 7/group). ***$p < 0.001$ compared with the MCAO group. (For interpretation of the references to colour in this figure legend, the reader is referred to the web version of this article.)

ischemic stroke rats [44]. In the current study, we found a markedly increase in both extracellular and intracellular ROS after APP treatment. Furthermore, scavenger of ROS significantly abolished the APP preconditioning induced neuroprotective effects against OGD, indicating that the ROS of APP productions was a main contributor for its neuroprotective effects.

Then, the relationship of ROS and autophagy was further studied. ROS is a critical molecule involved in autophagy regulation [45]. Nevertheless, long-term stimulation with ROS results in cell death. Our results also showed that long exposure to APP would reduce cell viability. Previous studies have indicated that ROS can regulate autophagy-related protein activation by directly targeting cysteine protease HsAtg4 and stimulate autophagy for cell survival and protection [46]. A recent study found that the transcription factor EB (TFEB) could be oxidized by ROS at a conserved Cys212 residue, and this oxidation enabled TFEB translocation to nuclei for active transcription of a battery of autophagic and lysosomal genes, which further activated autophagy and lysosome biogenesis [47]. In our current study, effects of ROS from APP preconditioning on cell autophagy were confirmed using the ROS scavenger NAC. We found that NAC abolished the autophagy and cytoprotection induced by APP treatment, suggesting that among the many active species produced by APP, ROS was the main one causing cellular autophagy and cytoprotective effects.

It should be noted that, the active species composition of plasma is very complex. Although some molecules or atoms in the excited state can form ROS or RNS by interacting with liquids or cells, there are also other kinds of active species, such as atoms, molecules in other valence states, as well as free electrons whose biological functions remain unknown. In this study, the extracellular and intracellular ROS generated by the plasma treatment was much higher than RNS. Meanwhile, the ROS inhibitors or ROS inhibitors combined with RNS inhibitors abolished the activation of ROS/AMPK/mTOR pathway and neuroprotective effects induced by plasma. RNS inhibitors had no effect on these effects. Therefore, we speculate that ROS played a dominant role of the cytoprotective effect against OGD injuries during APP preconditioning. We also hypothesize that the biological function of plasma is the result of the joint action of various species. Especially in the in vivo studies, although our experiments confirmed the therapeutic effect of plasma inhalation on MCAO model rats, the specific mechanism and the role of other reactive species are still unclear, and future studies will more concentrate on that.

The downstream signal pathway of ROS was further studied. AMPK, which is a regulator of metabolic abnormality, is a serine–threonine kinase [48]. AMPK refers to a pro-survival kinase that is activated during cellular stress to regulate numerous signaling intermediates and transcription factors, leading to the increased cell survival and proliferation [49]. AMPK is activated under energy stress conditions with an elevation in the AMP/ATP ratio, which can therefore hinder mTOR and initiating autophagy [50]. AMPK activation has been shown to be neuroprotective depending upon the neural cell types, the nature of insults, and the intensity and duration of AMPK activation [51]. Meanwhile, AMPK is a downstream signal factor for ROS. It has been reported that mitochondrial ROS activate AMPK, which reciprocally limits mitochondrial ROS production through a PGC-1α-dependent antioxidant response and further regulates the Warburg metabolism [52]. Previously, it has been demonstrated by Choi et al that AMPK could be activated by H_2O_2 by AMPK α1 threonine 172 phosphorylation [53]. A former study indicated that ROS regulates the activity of the survival kinase AMPK and autophagy in endothelial cells [54]. Meanwhile, another study also showed that autophagy activated by PAPR-1-LKB1–AMPK–mTOR pathway could protect endothelial cells, which was dependent on ROS generation [55]. In our current study, SH-SY5Y cells were pretreated with AMPK inhibitor CC before APP preconditioning, and the results showed that CC inhibited cell autophagy and abolished the cytoprotective effect of APP preconditioning against OGD injuries. Meanwhile, CC reduced p-AMPK/t-AMPK ratio and increased p-mTOR/mTOR ratio which was induced by APP preconditioning.

In MCAO models, the AMPK/MTOR pathway has been shown to exert vital roles in cellular responses to ischemic injury and potential therapeutic interventions. Studies have shown that AMPK activation could maintain cellular energy homeostasis under ischemic conditions by promoting glucose uptake, enhancing mitochondrial function, and reducing oxidative stress, which contribute to neuroprotection and the improved outcomes post-ischemia [56]. However, the function of mTOR in MCAO models was more controversial. Several studies of brain ischemia have reported a reduction in mTOR activity after ischemic damage, accompanied by neuronal death and neurological deficits. Activation of mTOR can promote neuronal survival and diminish ischemic damage, which may aid in tissue repair and recovery [57]. However, it is also found that pharmacological inhibition of mTOR could also be beneficial for brain ischemia, not only via neuronal autophagy but also through its broader effects on the neurovascular unit or attenuation of neuroinflammation [58,59]. Our current study only investigated the regulation of APP treatment on autophagy and AMPK/MTOR pathway in vitro, which is a limitation of our study. Our future study will pay more attention on the expression of ROS/RNS and AMPK/MTOR pathway by APP or inhibitors treatment in brain tissues of MCAO rats.

The application time of APP treatment for the in vitro and in vivo studies was different in the present study. Since the biomedical applications of plasma are mainly based on the ROS and RNS production by plasma treatment and the cellular OGD injury is accompanied by the elevation of intracellular ROS/RNS and can directly result in oxidative stress injury, postconditioning of OGD injured cells with APP may further increase the content of intracellular ROS/RNS and exacerbate the oxidative stress injury of cells. Therefore, in the in vitro studies, cells were pretreated with APP and we found that plasma preconditioning could reduce OGD induced cell apoptosis by activating ROS/AMPK/mTOR pathway and autophagy. During the in vivo study, we considered the application way of plasma in clinical ischemic stroke treatment, so the postconditioning was applied for MCAO rats. Rats received nasal inhalation of plasma at 60 min after MCAO, which could reduce the brain reperfusion injuries, suggesting the prospect of plasma in clinical ischemic stroke treatment. On the other hand, preconditioning of plasma in vivo may also be important for its application. As suggested by our in vitro studies, daily inhalation plasma may be a preventive or healthcare tool for cerebral ischemic injury, but the plasma generation and treatment conditions need to be further optimized, which is an important direction for our future research.

In summary, a helium APP device is used for the treatment of SH-SH5Y cells to evaluate the neuroprotective effects of APP preconditioning against OGD injuries with the optimized parameters. APP preconditioning can decrease cell apoptosis caused by OGD in a dose-dependent manner. Further studies confirm that the ROS of APP productions is the main contributor to the cytoprotective effect, which was regulated by the activation of cell autophagy and ROS/ AMPK/mTOR pathway. Although more work is still needed in our future studies, this study provides novel insights and practical methods for the uses of atmospheric pressure plasma in the ischemic disorder treatments.

CRediT authorship contribution statement

Xu Yan: Writing – original draft. **Qi Zhang:** Writing – original draft. **Yixiao Liu:** Methodology. **Yuqi Guo:** Software. **Zhongfang Shi:** Software. **Lixin Xu:** Methodology. **Zilan Xiong:** Writing – review & editing. **Jiting Ouyang:** Writing – review & editing. **Ye Chen:** Writing – review & editing. **Kostya (Ken) Ostrikov:** Writing – review & editing.

Declaration of competing interest

The authors declare that they have no known competing financial interests or personal relationships that could have appeared to influence

the work reported in this paper.

Data availability

No data was used for the research described in the article.

Acknowledgments

This work was funded by the National Natural Science Foundation of China (Grant Nos. 52077006 and 51707012), Beijing Natural Science Foundation (No.7232332) and Medical Innovation Capability Improvement Plan of Capital Medical University.

References

[1] J. Meschia, T. Brott, Ischaemic stroke, Eur. J. Neurol. 25 (1) (2018) 35–40.
[2] C. Qin, S. Yang, Y.-H. Chu, H. Zhang, X.-W. Pang, L. Chen, L.-Q. Zhou, M. Chen, D.-S. Tian, W. Wang, Signaling pathways involved in ischemic stroke: molecular mechanisms and therapeutic interventions, Signal Transduct. Target. Ther. 7 (1) (2022) 215.
[3] G.J. Hankey, Stroke, Lancet 389 (10069) (2017) 641–654.
[4] S.E. Thomas, N. Plumber, P. Venkatapathappa, V. Gorantla, A review of risk factors and predictors for hemorrhagic transformation in patients with acute ischemic stroke, Int. J. Vasc. Med. 2021 (2021).
[5] J. Liu, F. Kuang, G. Kroemer, D.J. Klionsky, R. Kang, D. Tang, Autophagy-dependent ferroptosis: machinery and regulation, Cell Chem. Biol. 27 (4) (2020) 420–435.
[6] W. Chen, Y. Sun, K. Liu, X. Sun, Autophagy: a double-edged sword for neuronal survival after cerebral ischemia, Neural Regen. Res. 9 (12) (2014) 1210.
[7] J. Du, Y. Li, W. Zhao, Autophagy and myocardial ischemia, Autophagy: Biology and Diseases: Clinical Science (2020) 217–222.
[8] T. Zhang, J. Guo, J. Gu, K. Chen, H. Li, J. Wang, Protective role of mTOR in liver ischemia/reperfusion injury: involvement of inflammation and autophagy, Oxidative Med. Cell. Longev. 2019 (2019).
[9] X. Zhang, M. Wei, J. Fan, W. Yan, X. Zha, H. Song, R. Wan, Y. Yin, W. Wang, Ischemia-induced upregulation of autophagy preludes dysfunctional lysosomal storage and associated synaptic impairments in neurons, Autophagy 17 (6) (2021) 1519–1542.
[10] S.F. Nabavi, A. Sureda, A. Sanches-Silva, K. Pandima Devi, T. Ahmed, M. Shahid, E. Sobarzo-Sánchez, M. Dacrema, M. Daglia, N. Braidy, Novel therapeutic strategies for stroke: the role of autophagy, Crit. Rev. Clin. Lab. Sci. 56 (3) (2019) 182–199.
[11] S. Bekeschus, Medical gas plasma technology: roadmap on cancer treatment and immunotherapy, Redox Biol 65 (2023) 102798.
[12] Z. Chen, G. Chen, R. Obenchain, R. Zhang, F. Bai, T. Fang, H. Wang, Y. Lu, R. E. Wirz, Z. Gu, Cold atmospheric plasma delivery for biomedical applications, Mater. Today 54 (2022) 153–188.
[13] M. Laroussi, Sterilization of contaminated matter with an atmospheric pressure plasma, Ieee T Plasma Sci 24 (3) (1996) 1188–1191.
[14] M.G. Kong, G. Kroesen, G. Morfill, T. Nosenko, T. Shimizu, J.V. Dijk, J. L. Zimmermann, Plasma medicine: an introductory review, New J. Phys. 11 (11) (2009) 115012.
[15] C. Man, C. Zhang, H. Fang, R. Zhou, B. Huang, Y. Xu, X. Zhang, T. Shao, Nanosecond-pulsed microbubble plasma reactor for plasma-activated water generation and bacterial inactivation, Plasma Process. Polym. 19 (6) (2022) 2200004.
[16] E.H. Choi, H.S. Uhm, N.K. Kaushik, Plasma bioscience and its application to medicine, AAPPS Bull. 31 (1) (2021) 10.
[17] X. Yan, J. Ouyang, C. Zhang, Z. Shi, B. Wang, K.K. Ostrikov, Plasma medicine for neuroscience—an introduction, Chinese Neurosurgical Journal 5 (1) (2019) 1–8.
[18] L. Lin, M. Keidar, A map of control for cold atmospheric plasma jets: from physical mechanisms to optimizations, Appl. Phys. Rev. 8 (1) (2021) 011306.
[19] X. Yan, B. Yang, J. Ouyang, C. Zhang, Y. Lai, Z. Shi, R. Han, W. Zhang, F. Yuan, K. Ostrikov, Mechanisms of atmospheric pressure plasma protection of neuronal cells under simulated ischemic stroke conditions, AIP Adv. 12 (2) (2022) 025114.
[20] X. Yan, C. Zhang, J. Ouyang, Z. Shi, Y. Chen, R. Han, W. Zhang, F. Yuan, K. K. Ostrikov, Atmospheric pressure plasma treatments protect neural cells from ischemic stroke-relevant injuries by targeting mitochondria, Plasma Process. Polym. 17 (10) (2020) e2000063.
[21] M. Tian, M. Qi, Z. Liu, D. Xu, H. Chen, M.G. Kong, Cold atmospheric plasma elicits neuroprotection against glutamate excitotoxicity by activating cellular antioxidant defense, Plasma Chem Plasma P (2021) 1–10.
[22] Y. Chen, B. Yang, Y. Liu, L. Xu, Z. Shi, Y. Liu, R. Han, F. Yuan, J. Ouyang, X. Yan, Application of an Atmospheric Pressure Plasma Jet in a Rat Model of Ischaemic Stroke: Design, Optimisation, and Characteristics, High Voltage, 2022.
[23] Y. Chen, B. Yang, L. Xu, Z. Shi, R. Han, F. Yuan, J. Ouyang, X. Yan, K.K. Ostrikov, Inhalation of atmospheric-pressure gas plasma attenuates brain infarction in rats with experimental ischemic stroke, Front. Neurosci. 16 (2022).
[24] A.L. Garner, T.A. Mehlhorn, A review of cold atmospheric pressure plasmas for trauma and acute care, Front. Phys. 9 (2021) 774.
[25] D. Yan, A. Malyavko, Q. Wang, K. Ostrikov, J.H. Sherman, M. Keidar, Multi-modal biological destruction by cold atmospheric plasma: capability and mechanism, Biomedicines 9 (9) (2021) 1259.
[26] D. Wang, J. Zhang, L. Cai, X. Dai, Cold atmospheric plasma conveys selectivity against hepatocellular carcinoma cells via triggering EGFR(Tyr1068)-mediated autophagy, Front. Oncol. 12 (2022) 895106.
[27] G.E. Conway, Z. He, A.L. Hutanu, G.P. Cribaro, E. Manaloto, A. Casey, D. Traynor, V. Milosavljevic, O. Howe, C. Barcia, J.T. Murray, P.J. Cullen, J.F. Curtin, Cold atmospheric plasma induces accumulation of lysosomes and caspase-independent cell death in U373MG glioblastoma multiforme cells, Sci. Rep. 9 (1) (2019) 12891.
[28] Y. Wu, J. Liu, L. Gao, Y. Ma, G. Xu, X. Li, Y. Hao, X. Shi, G.-J. Zhang, Helium low temperature plasma induced HepG2 cells autophagy through ROS-mediated PI3K/AKT/mTOR/P70s6k signaling pathway, AIP Adv. 9 (9) (2019) 095034.
[29] L. Galluzzi, J.M. Bravo-San Pedro, B. Levine, D.R. Green, G. Kroemer, Pharmacological modulation of autophagy: therapeutic potential and persisting obstacles, Nat. Rev. Drug Discov. 16 (7) (2017) 487–511.
[30] P. Wang, B.-Z. Shao, Z. Deng, S. Chen, Z. Yue, C.-Y. Miao, Autophagy in ischemic stroke, Prog. Neurobiol. 163-164 (2018) 98–117.
[31] S. Saleem, Apoptosis, autophagy, necrosis and their multi galore crosstalk in neurodegeneration, Neuroscience 469 (2021) 162–174.
[32] R. Gupta, R.K. Ambasta, P. Kumar, Autophagy and apoptosis cascade: which is more prominent in neuronal death? Cell. Mol. Life Sci. 78 (24) (2021) 8001–8047.
[33] C. Porrini, N. Ramarao, S.-L. Tran, Dr. NO and Mr. Toxic–the versatile role of nitric oxide, Biol. Chem. 401 (5) (2020) 547–572.
[34] S.Y. Park, M.Y. Park, H.G. Park, K.J. Lee, M.S. Kook, W.J. Kim, J.Y. Jung, Nitric oxide-induced autophagy and the activation of activated protein kinase pathway protect against apoptosis in human dental pulp cells, Int. Endod. J. 50 (3) (2017) 260–270.
[35] M.K. Shirazi, A. Azarnezhad, M.F. Abazari, M. Poorebrahim, P. Ghoraeian, N. Sanadgol, H. Bokharaie, S. Heydari, A. Abbasi, S. Kabiri, M.N. Aleagha, S. E. Enderami, A.S. Dashtaki, H. Askari, The role of nitric oxide signaling in renoprotective effects of hydrogen sulfide against chronic kidney disease in rats: involvement of oxidative stress, autophagy and apoptosis, J. Cell. Physiol. 234 (7) (2019) 11411–11423.
[36] J.-K. Shin, J.-W. Kang, S.-M. Lee, Enhanced nitric oxide-mediated autophagy contributes to the hepatoprotective effects of ischemic preconditioning during ischemia and reperfusion, Nitric Oxide 58 (2016) 10–19.
[37] H. Arimoto, D. Takahashi, 8-nitro-cGMP: a novel protein-reactive cNMP and its emerging roles in autophagy, Handb. Exp. Pharmacol. 238 (2017) 253–268.
[38] W.R. Williams, Contributors to Cancer susceptibility, development and treatment: cyclic nucleotides, steroids and autophagy modulators, J. Biosci. and Med. 10 (2) (2022) 65–86.
[39] E. Martínez-Martínez, P. Atzei, C. Vionnet, C. Roubaty, S. Kaeser-Pebernard, R. Naef, J. Dengjel, A dual-acting nitric oxide donor and phosphodiesterase 5 inhibitor activates autophagy in primary skin fibroblasts, Int. J. Mol. Sci. 23 (12) (2022) 6860.
[40] H. Sies, V.V. Belousov, N.S. Chandel, M.J. Davies, D.P. Jones, G.E. Mann, M. P. Murphy, M. Yamamoto, C. Winterbourn, Defining roles of specific reactive oxygen species (ROS) in cell biology and physiology, Nat. Rev. Mol. Cell Biol. 23 (7) (2022) 499–515.
[41] H. Sies, D.P. Jones, Reactive oxygen species (ROS) as pleiotropic physiological signalling agents, Nat. Rev. Mol. Cell Biol. 21 (7) (2020) 363–383.
[42] M. Armogida, R. Nisticò, N.B. Mercuri, Therapeutic potential of targeting hydrogen peroxide metabolism in the treatment of brain ischaemia, Br. J. Pharmacol. 166 (4) (2012) 1211–1224.
[43] C. Su, F. Sun, R.L. Cunningham, N. Rybalchenko, M. Singh, ERK5/KLF4 signaling as a common mediator of the neuroprotective effects of both nerve growth factor and hydrogen peroxide preconditioning, Age 36 (2014) 1–17.
[44] M. Simerabet, E. Robin, I. Aristi, S. Adamczyk, B. Tavernier, B. Vallet, R. Bordet, G. Lebuffe, Preconditioning by an in situ administration of hydrogen peroxide: involvement of reactive oxygen species and mitochondrial ATP-dependent potassium channel in a cerebral ischemia–reperfusion model, Brain Res. 1240 (2008) 177–184.
[45] J. Zhou, X.-Y. Li, Y.-J. Liu, J. Feng, Y. Wu, H.-M. Shen, G.-D. Lu, Full-coverage regulations of autophagy by ROS: from induction to maturation, Autophagy 18 (6) (2022) 1240–1255.
[46] R. Scherz-Shouval, E. Shvets, E. Fass, H. Shorer, L. Gil, Z. Elazar, Reactive oxygen species are essential for autophagy and specifically regulate the activity of Atg4, EMBO J. 26 (7) (2007) 1749–1760.
[47] H. Wang, N. Wang, D. Xu, Q. Ma, Y. Chen, S. Xu, Q. Xia, Y. Zhang, J.H. Prehn, G. Wang, Oxidation of multiple MiT/TFE transcription factors links oxidative stress to transcriptional control of autophagy and lysosome biogenesis, Autophagy 16 (9) (2020) 1683–1696.
[48] C. Rodríguez, M. Muñoz, C. Contreras, D. Prieto, AMPK, metabolism, and vascular function, FEBS J. 288 (12) (2021) 3746–3771.
[49] C. Garza-Lombó, A. Schroder, E.M. Reyes-Reyes, R. Franco, mTOR/AMPK signaling in the brain: cell metabolism, proteostasis and survival, Current Opinion in Toxicology 8 (2018) 102–110.
[50] Y. Li, Y. Chen, AMPK and autophagy, Autophagy: Biology and Diseases: Basic Science (2019) 85–108.
[51] R. Muraleedharan, B. Dasgupta, AMPK in the brain: its roles in glucose and neural metabolism, FEBS J. 289 (8) (2022) 2247–2262.
[52] R.C. Rabinovitch, B. Samborska, B. Faubert, E.H. Ma, S.-P. Gravel, S. Andrzejewski, T.C. Raissi, A. Pause, J. St.-Pierre, R.G. Jones, AMPK maintains cellular metabolic homeostasis through regulation of mitochondrial reactive oxygen species, Cell Rep. 21 (1) (2017) 1–9.

[53] S.-L. Choi, S.-J. Kim, K.-T. Lee, J. Kim, J. Mu, M.J. Birnbaum, S.S. Kim, J. Ha, The regulation of AMP-activated protein kinase by H2O2, Biochem. Biophys. Res. Commun. 287 (1) (2001) 92–97.
[54] E. Shafique, W.C. Choy, Y. Liu, J. Feng, B. Cordeiro, A. Lyra, M. Arafah, A. Yassin-Kassab, A.V. Zanetti, R.T. Clements, Oxidative stress improves coronary endothelial function through activation of the pro-survival kinase AMPK, Aging (Milano) 5 (7) (2013) 515–530.
[55] G.-h. Li, X.-l. Lin, H. Zhang, S. Li, X.-l. He, K. Zhang, J. Peng, Y.-l. Tang, J.-f. Zeng, Y. Zhao, Ox-Lp (a) transiently induces HUVEC autophagy via an ROS-dependent PAPR-1-LKB1–AMPK–mTOR pathway, Atherosclerosis 243(1) (2015) 223–235.
[56] M.D.A. Paskeh, A. Asadi, S. Mirzaei, M. Hashemi, M. Entezari, R. Raesi, K. Hushmandi, A. Zarrabi, Y.N. Ertas, A.R. Aref, Targeting AMPK signaling in ischemic/reperfusion injury: from molecular mechanism to pharmacological interventions, Cell. Signal. 94 (2022) 110323.
[57] M. Villa-González, G. Martín-López, M.J. Pérez-Álvarez, Dysregulation of mTOR signaling after brain ischemia, Int. J. Mol. Sci. 23 (5) (2022) 2814.
[58] G. Hadley, D.J. Beard, Y. Couch, A.A. Neuhaus, B.A. Adriaanse, G.C. DeLuca, B. A. Sutherland, A.M. Buchan, Rapamycin in ischemic stroke: old drug, new tricks? J. Cereb. Blood Flow Metab. 39 (1) (2019) 20–35.
[59] M. Villa-González, M. Rubio, G. Martín-López, P.R. Mallavibarrena, L. Vallés-Saiz, D. Vivien, F. Wandosell, M.J. Pérez-Álvarez, Pharmacological inhibition of mTORC1 reduces neural death and damage volume after MCAO by modulating microglial reactivity, Biol. Direct 19 (1) (2024) 26.